Fuel 324 (2022) 124748

Contents lists available at ScienceDirect

Fuel

journal homepage: www.elsevier.com/locate/fuel

Full Length Article

Low-speed performance compensation of a turbocharged natural gas engine by intake strategy optimization

Kun Luo [a], Yongcheng Huang [a,*], Zhiyu Han [b], Yaoting Li [a], Yongsheng Shi [c], Wei Liu [c], Chenglong Tang [a,*]

[a] School of Energy and Power Engineering, Xi'an Jiaotong University, Xi'an 710049, PR China
[b] College of Automotive Studies, Tongji University, Shanghai 201804, PR China
[c] Jiangsu Smapow Engine Co.Ltd., Huai'an, Jiangsu 223005, PR China

ARTICLE INFO

Keywords:
Low-speed performance
Natural gas engine
Hierarchical 1D/3D approach
Asynchronized intake strategy
Turbocharging

ABSTRACT

Power output at the low engine speed is limited for natural gas engines, even though the turbocharging technology is used. In this paper, the intake system of a turbocharged spark-ignition natural gas engine with 4 valves (2 intake valves and 2 exhaust valves) was optimized by considering the intake strategy effects on the engine torque output and fuel economy improvement. Firstly, a 1D numerical model with hierarchical 1D/3D approach based on GT-SUITE was developed and validated against the experimental data of engine torque and fuel consumption rate. This approach combined detailed analysis of in-cylinder flow, charge movement and combustion. Secondly, different intake strategies were designed and their effects on the intake mass flow rate and in-cylinder mass during the intake process, the swirl flow, tumble ratio and the turbulent kinetic energy during the compression process, the flame propagation and temperature distribution evolution after the spark ignition, and the pressure and heat release rate were numerically investigated. The results showed that compared with the original intake strategy, the asynchronized intake strategy (the intake valves close earlier and the intake valve lifts are reduced, while two intake valves have different intake strategy) reduces the backflow in the end of intake stroke, improves the in-cylinder swirl flow, increases the maximum heat release rate and shortens the combustion duration, and it is believed to be the optimized intake strategy. Finally, different cam profiles corresponding to the numerically designed intake strategies were applied to the bench test engine and the dyno experiments showed that the optimized intake strategy improves the torque and reduces the brake specific fuel consumption by 41.42% and 8.1% respectively at a low engine speed of 1200 rpm.

1. Introduction

Natural gas has many advantages when used as an alternative engine fuel for gasoline and diesel, such as lower cost and less pollutant emissions [1,2]. In addition, natural gas has a higher octane number (120–130) which allows the engine to operate at a higher compression ratio and thus achieve higher thermal efficiency [3]. CO_2 emissions of natural gas engines can be reduced by more than 20% when compared with gasoline engines at an equal power output [4]. Therefore, natural gas engines are becoming increasingly attractive, especially for commercial vehicles and urban public transportation [5].

However, natural gas engines have typically lower torque output compared to gasoline engines [6]. Firstly, when the port fuel injection (PFI) natural gas engines operate at stoichiometric conditions, natural gas occupies about 10% more volume of the intake air compared to gasoline engines, which reduces the chemical energy input per cycle under a fixed engine displacement [7]. In addition, the lack of latent heat of evaporation decreases the volumetric efficiency of natural gas engines. Thus, the volumetric efficiency of the PFI natural gas engine is typically 8% lower than that of the gasoline engine [8,9]. In order to increase the torque output of natural gas engines, one prevalent

Abbreviations: PFI, port fuel injection; EGR, exhaust gas recirculation; SI, spark ignited; WOT, wide open throttle; CNG, compressed natural gas; IVO, intake valve open; IVC, intake valve close; EVO, exhaust valve open; EVC, exhaust valve close; TDC, top dead center; BDC, bottom dead center; ATDC, after top dead center; BTDC, before Top dead center; CA, crank angle; CFD, computational fluid dynamics; RNG, re-normalization group; TKE, turbulent kinetic energy; BSFC, brake fuel consumption rate.

* Corresponding authors.
E-mail addresses: huangyc@xjtu.edu.cn, huangyc@xjtu.edu.cn (Y. Huang), chenglongtang@mail.xjtu.edu.cn (C. Tang).

https://doi.org/10.1016/j.fuel.2022.124748
Received 12 September 2021; Received in revised form 31 May 2022; Accepted 1 June 2022
Available online 8 June 2022

Nomenclature

M_e	Entrained mass of the unburned mixture
A_f	Proportion of the flame surface
S_T	Turbulent flame speed
u'	Turbulent intensity
R_f	Radius of the flame
M_b	Mass of burnt mixture gas
C_λ	Calibration parameter of Taylor microscale
Re_t	Reynolds number
B_m	Maximum laminar speed
ϕ	In-cylinder equivalence ratio
T_u	Temperature of unburned mixture
p	In-cylinder pressure
α	Temperature exponent
$\dot{q}$ *	Heat flux
A_w	Proportion of the wall
T	In-cylinder temperature
ω	Average velocity of mixture gas
k	Turbulent kinetic energy
ρ_u	Density of the unburned mixture
S_L	Laminar flame speed
C_s	Calibration parameter of the turbulent flame speed
C_k	Calibration parameter of flame kernel growth
L_t	Turbulent length scale
τ	Characteristic burning time
λ	Taylor microscale length
μ	Viscosity coefficient
B_ϕ	Laminar speed roll-off value
ϕ_m	Equivalence ratio at max engine speed
T_{ref}	Reference temperature (298 K)
p_0	Reference pressure (0.1 MPa)
β	Pressure exponent
C_q	Calibration parameter of heat transfer
h_c	Convective heat transfer coefficient
T_w	Temperature of the wall
K	Kinetic energy
ε	Turbulence integral length scale

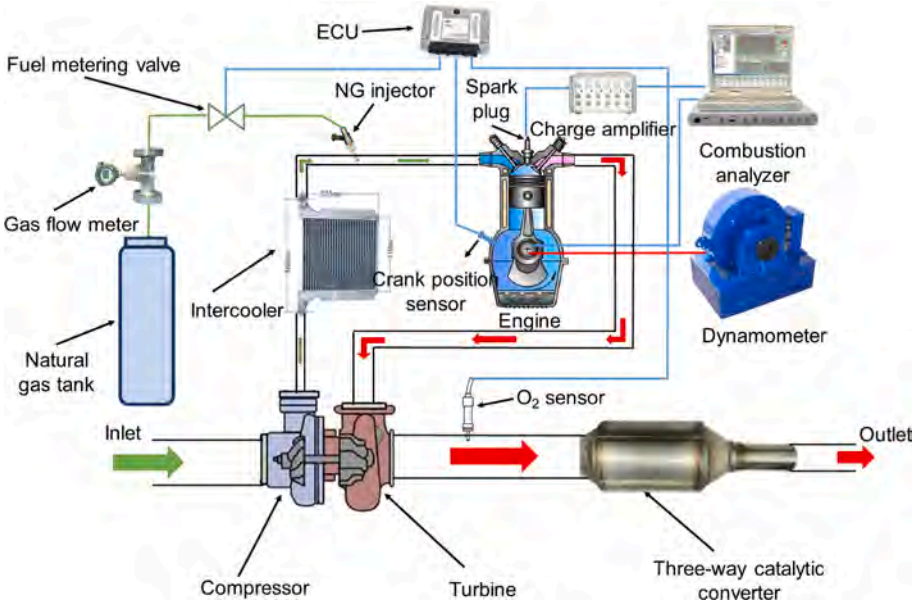

Fig. 1. Schematic diagram of the engine setup.

Table 1
Main specifications of the natural gas engine.

Items	Descriptions
Engine type	4-cylinder, 4-stroke, four valves per cylinder, nature gas engine
Cooling type	Water-cooling
Injection strategy	Port fuel injection
Charging strategy	Turbocharging and inter-cooling
Displacement	2.4 L
Bore × Stroke	87 mm × 100 mm
Compression ratio	9.6:1
Maximum power	131 kW @ 5200 rpm
Maximum torque	304 N·m @ 4000 rpm
Emission level	Euro VI

approach is to increase the density of intake air by supercharging [10] or turbocharging [11]. However, at low engine speeds, turbocharging is not feasible due to the low exhaust gas enthalpy. Supercharging can increase the density of intake air at low engine speeds, while mechanical compression consumes the crankshaft work. As such, low-speed engine power performance cannot be improved by the state-of-the-art turbocharging or supercharging techniques.

Several other approaches have been reported to boost the power performance of natural gas engines [12,13,14,15]. Luisi et al. [12] tested Miller cycle through late intake valve closure to achieve a shorter compression stroke and lower in-cylinder charge temperatures. A significant reduction in fuel consumption is realized at high load engine conditions. Ferrera et al. [13] investigated the side direct injection of compressed natural gas (CNG) effect on engine performance. Their numerical and experimental research both showed that the side direct injection of CNG can improve local mixture formation at the spark plug and therefore favors the ignition. In addition, compared with the PFI, the side direct injection increases the volumetric efficiency and the combustion rate of fuel, and thus leads to a better brake thermal efficiency. Zhang et al. [14] numerically investigated the effect of exhaust gas

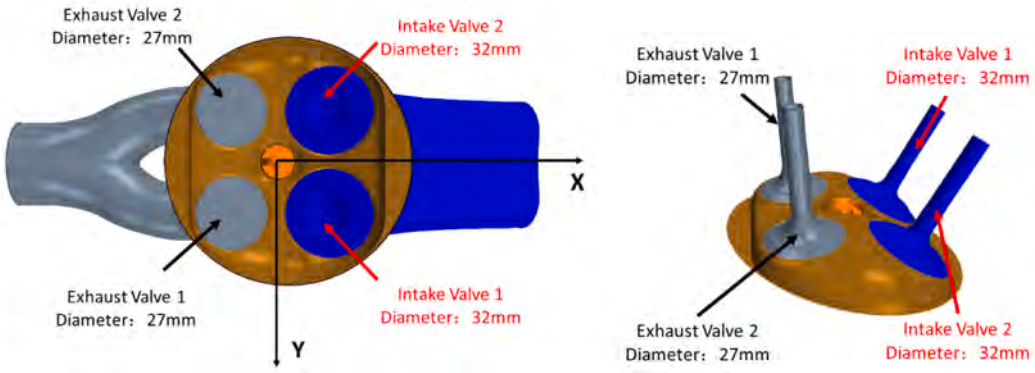

a) The structure diagram of four valves

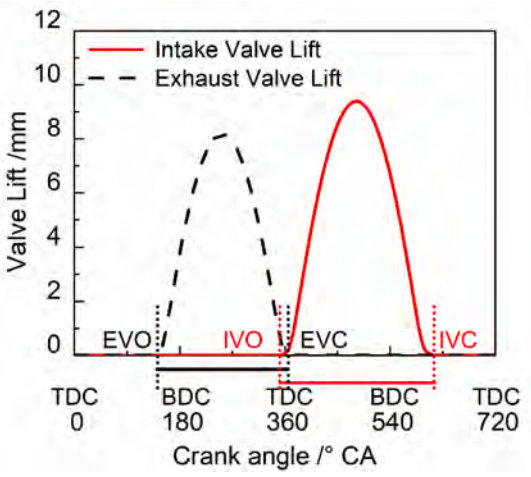

b) Intake valve lift and exhaust valve lift

Fig. 2. Original intake and exhaust strategy of the bench test engine.

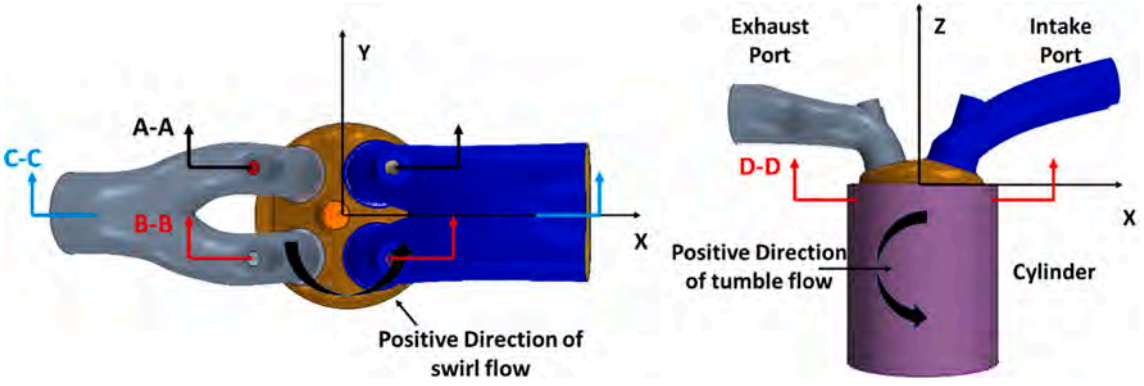

Fig. 3. Engine geometry domain for CFD simulation.

recirculation (EGR) strategies on the combustion performance of a heavy-duty high compression ratio natural gas engine. The simulation results show that at the low EGR ratio, the indicated thermal efficiency and specific fuel consumption remain basically unchanged. When the EGR ratio exceeds 20%, the indicated thermal efficiency decreases and the specific fuel consumption increases. Bhasker and Porpatham [15] studied the effects of hydrogen addition on the combustion and emission characteristics of a natural gas fueled spark ignition (SI) engine. They found that under wide open throttle (WOT) conditions at a fixed engine speed, hydrogen addition can significantly improve the performance and reduce the HC and NO_x emissions.

The intake strategy effects have also been investigated. For instance, Sabaruddin et al. [16] examined the gas exchange process and performance of a 4-valve SI engine by using different valve timings at different engine speeds. They observed that the gas exchange process is enhanced by increasing the volumetric efficiency with variable valve timing,

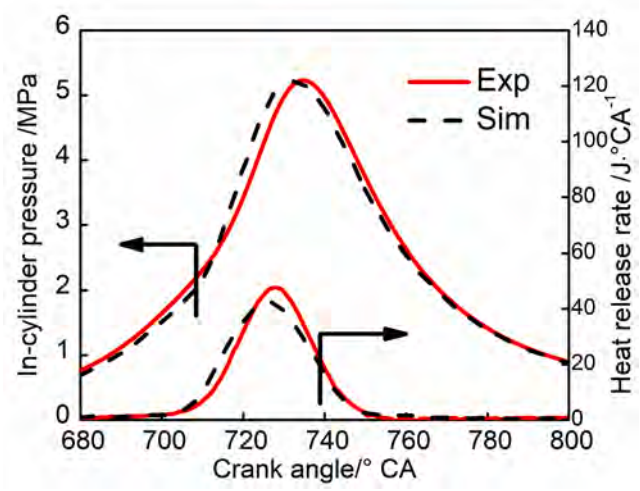

Fig. 4. Comparison of in-cylinder pressure and heat release rate at 1200 rpm.

Table 2
Model validation of ignition delay, CA50 and combustion duration.

Parameters	Experiment	Simulation
CA10/(°CA ATDC)	−5	−7.5
Ignition delay/(°CA)	15	12.5
CA50/(°CA ATDC)	7.5	6.5
CA90/(°CA ATDC)	20.5	21.2
Combustion duration/(°CA)	25.5	28.7

which leads to larger torque output, better efficiency, and lower fuel consumption. By using a 1D simulation model, Jung et al. [17] numerically investigated the influence of the intake valve close (IVC) on the engine performance and NOx emission of a natural gas diesel dual fuel engine at a fixed engine speed of 720 rpm with different engine loads. They found that for the dual fuel mode, advancement of IVC increases the brake power due to the reduced air fuel ratio and better gaseous fuel utilization. On the other hand, retarding IVC decreases NOx emissions because of the higher heat capacity of air due to more air induction. Lee et al. [18] experimentally studied the effect of tumble and swirl flows on the flame propagation in a four-valve SI engine at a fixed engine speed of 1250 rpm. It was found that a moderate organization of the tumble and swirl in the intake stroke increases the turbulent kinetic energy (TKE) at the time of ignition and thus enhances the subsequent flame propagation. Liu et al. [19] numerically designed the asynchronous valves timing (AVT) and synchronous valves timing (SVT) systems on a high-speed SI gasoline engine. Their computational fluid dynamics (CFD) simulation results showed that AVT scheme strengthens the in-cylinder flow during the intake stroke and increases the TKE near the top dead center (TDC), which is beneficial to the enhancement of flame propagation speed after the spark ignition. Their experimental results showed

Table 3
Mathematical expressions of the SITurb combustion model.

SITurb model [24,25]	NO. Eq. s
$\frac{dM_e}{dt} = \rho_u A_f (S_L + S_T)$	1
$S_T = C_s u' \left(1 - \frac{1}{1 + \frac{C_k R_f^2}{L_t^2}}\right)$	2
$\frac{dM_b}{dt} = \frac{M_e - M_b}{\tau}$	3
$\tau = \frac{\lambda}{S_L}$	4
$\lambda = \frac{C_s L_t}{\sqrt{Re_t}}$	5
$Re_t = \frac{\rho_u u' L_t}{\mu}$	6
$S_L = (B_m + B_\phi(\phi - \phi_m)^2)\left[\frac{T_u}{T_{ref}}\right]^\alpha \left[\frac{p}{p_0}\right]^\beta (1 - 2.06 R_f^{0.77DEM})$	7
Woschni heat-transfer model [6]	
$\dot{q}^* = C_q A_w h_c (T - T_w)$	8
$h_c = 3.26 B^{-0.2} p^{0.8} T^{-0.55} \omega^{0.8}$	9

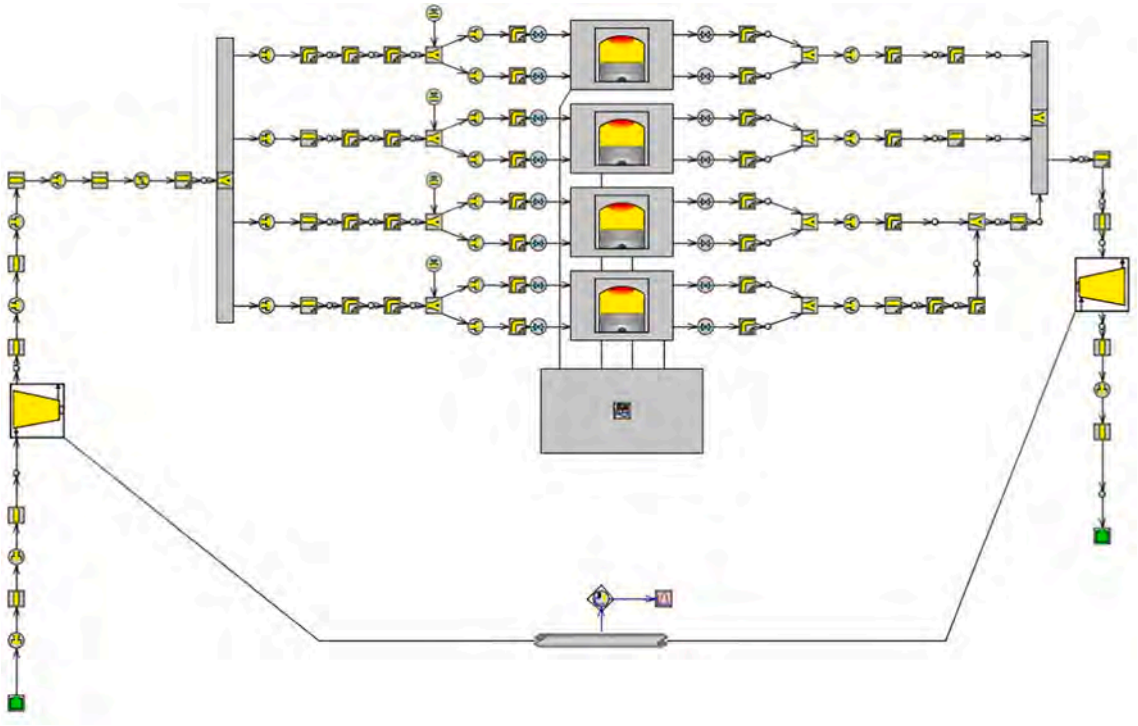

Fig. 5. 1D simulation model of the turbocharged spark ignition natural gas engine.

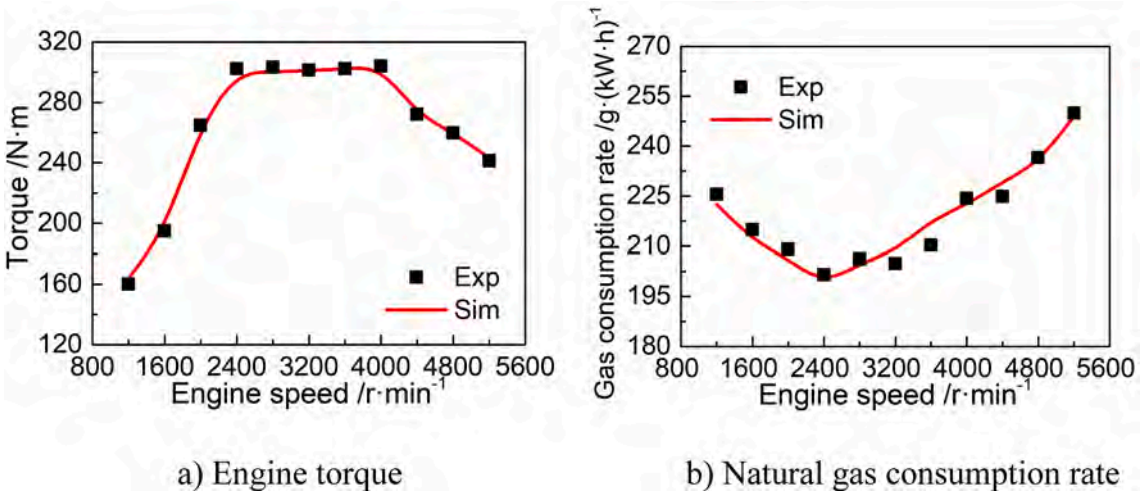

Fig. 6. The 1D model predicted and the measured engine torque and natural gas consumption rate.

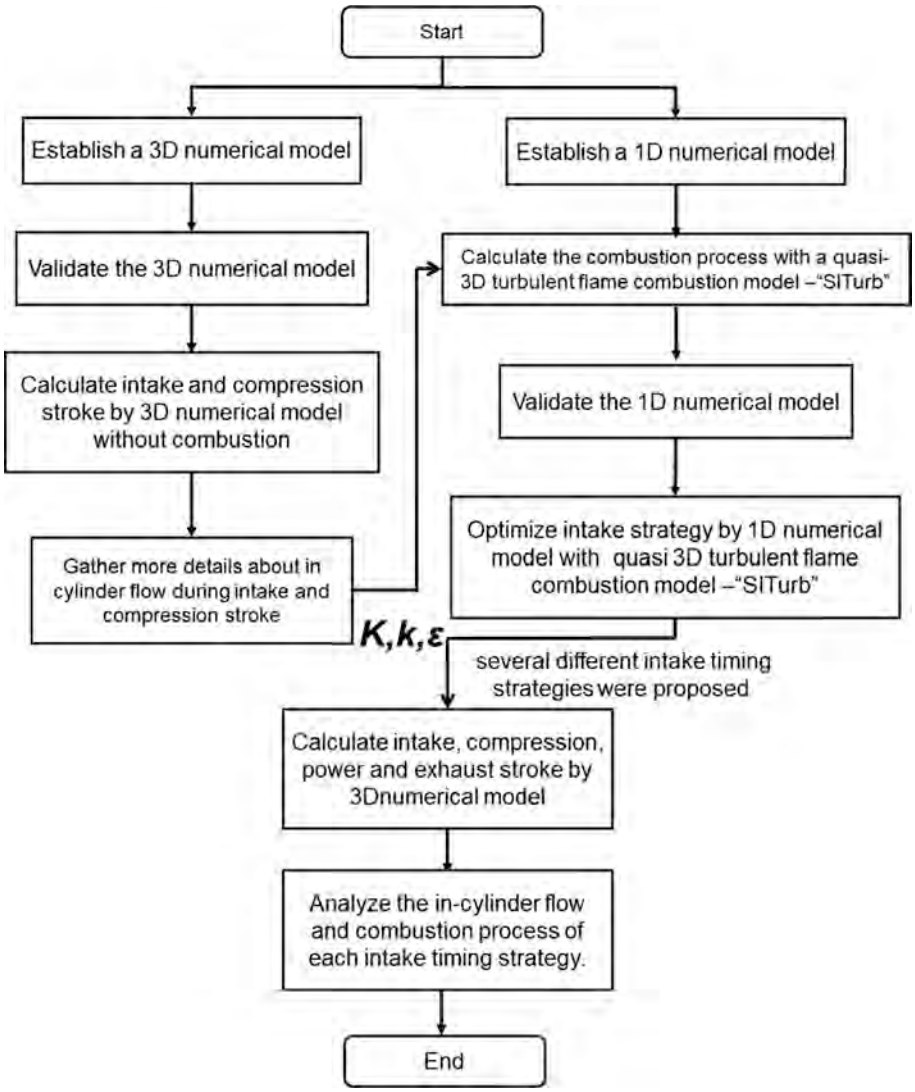

Fig. 7. Flowchart of the proposed hierarchical 1D/3D approach.

that the engine torque, fuel consumption, CO and HC emissions at full load under the designed AVT scheme are all lower than those under the SVT scheme.

Numerical simulation is both economical and effective in the optimization of the intake strategy. Different numerical models have been proposed for investigating the intake strategy effect on engine

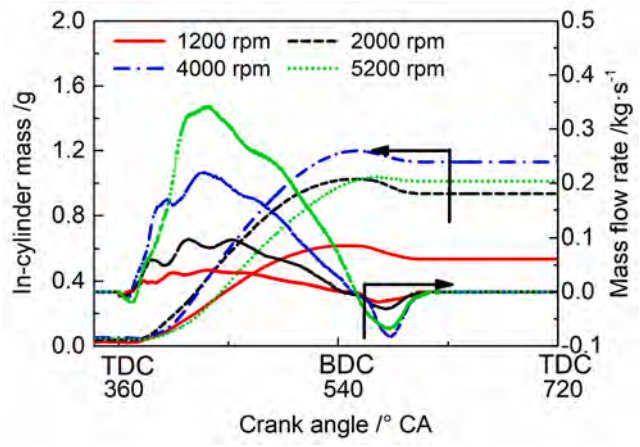

Fig. 8. Comparisons of the intake mass flow rate and in-cylinder mass changing with crank angle under different working conditions.

Table 4
The main parameters of different intake timing strategies.

Intake timing strategies		IVO/ °CA	IVC/°CA	Duration/ °CA	Maximum valve lift/mm
Synchronized	Case 1	351	615	264	9.39
	Case 2	351	615	264	8.59
	Case 3	351	591	240	8.59
Asynchronized	Case 4	351	591 (valve 1)	240 (valve 1)	8.59 (valve1)
			579 (valve 2)	228 (valve 2)	7.29 (valve 2)

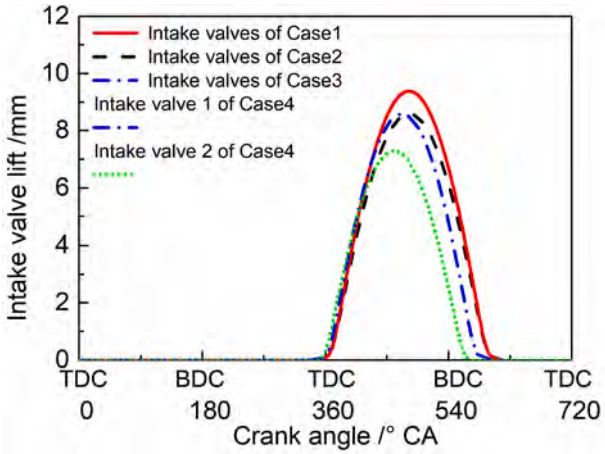

Fig. 9. The original (Case 1) and designed intake valve timing (Case 2 and Case 3: two intake valves are synchronized; case 4: intake valve 1 and 2 are asynchronized).

performance. For instance, Mirzaeian et al. [20] established a 1D phenomenological turbulence model, based on the coupling of the *K-k* and *k*-ε approaches and a predictive turbulent combustion model. The predictive 1D numerical model was validated against a downsized turbocharged SI engine.

The above studies [16,17] show that the intake strategy plays an important role in the engine performance. However, previous work [18–20] on the intake strategy optimization typically adopts the 1D numerical model, in which the in-cylinder flow behaviors during the intake and compression stroke, the flame propagation and in-cylinder temperature distribution during combustion cannot be resolved either. Thus, our first objective is to provide a link between the intake strategy and the heat release performance so as to understand the underlying mechanism for the engine performance enhancement. We will apply the hierarchical 1D/3D model approach [20] to the target turbocharged natural gas engine and by doing so the simulation of in-cylinder flow and combustion can be resolved. The numerical approach is firstly validated against the torque and fuel consumption of our bench test engine. Subsequently, by using the validated numerical approach, the in-cylinder flow and combustion behaviors, and the engine performances under different intake strategies are predicted and compared. As such, an optimized intake strategy design will be proposed. Finally, based on the numerical predictions, we modified the cam profile by applying different intake strategy designs and compared the corresponding engine performances, especially at the low engine speed. Our ultimate goal is to compensate the low-speed performance of a turbocharged natural gas engine by intake strategy optimization.

2. Experimental and numerical specifications

2.1. Experiments

2.1.1. Experimental system and procedure

Engine test rig is sketched in Fig. 1. An electric dynamometer (CAC160) is used to measure the engine speed and torque. The intake air flow rate was measured by a gas flow meter (ToCeil20N100) with an accuracy of ± 1%, and the natural gas consumption rate was measured by a gas flow meter (DMF-1-2-A) with the accuracy of ± 0.2%. The intake pressure and temperature, the exhaust pressure and temperature, and in-cylinder pressure over the whole cycle, were recorded for engine performance analysis. The in-cylinder pressure was recorded by a piezoelectric pressure transducer (Kistler 6125A). The environment temperature was controlled at 25 °C ± 1 °C during the engine test. Pressure data of 100 consecutive cycles were collected for average to calculate the heat release rate.

2.1.2. Test engine specification

The bench test engine is optimized from a gasoline engine. The base engine in this work is a 4-cylinder turbocharged SI natural gas engine, provided by China Smapow Engine Company. The base natural gas engine adopts a tangential intake port, which forms a strong tumble during the intake stroke, and employs the turbocharging technology to increase the density of intake air. The detailed engine dimensions and other information are provided in Table 1.

2.1.3. Original intake and exhaust strategy

The structure diagram, original intake and exhaust valve lift as a function of the crank angle of the four valves are presented in Fig. 2. The exhaust valves open at 142° CA (exhaust valve open, EVO) and close at 366° CA (exhaust valve close, EVC). The maximum exhaust valve lift is 8.18 mm. The intake valves open at 351° CA (intake valve open, IVO) and close at 615° CA (intake valve close, IVC). The maximum intake valve lift is 9.39 mm.

2.2. Numerical approach

2.2.1. 3D numerical model and validation

The commercial computational fluid dynamics (CFD) software STAR-CD was used to establish the 3D numerical model for the SI natural gas engine. Fig. 3 shows the engine geometry domain for numerical simulation. The positive directions of the tumble flow and swirl flow, and their coordinate system are illustrated. The grid consists of about 750,000 cells at the top dead center and about 1,600,000 cells at the bottom dead center. The CFD calculation was performed from 300° CA

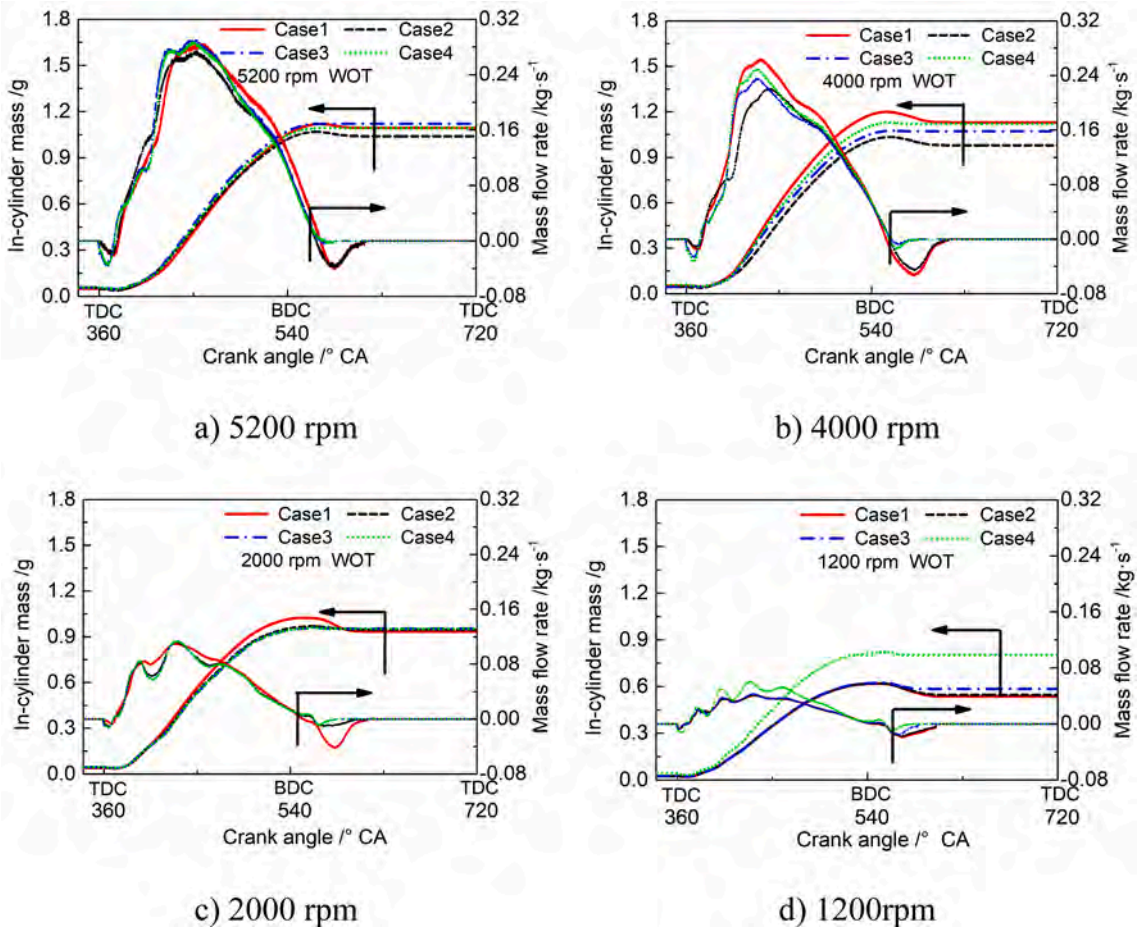

Fig. 10. Effect of the intake strategy on the instant mass flow rate and in-cylinder mass at different engine speeds.

to 900° CA. The Reynolds-averaged Naiver-Stokes (RANS) approach [21] was applied for calculating the in-cylinder turbulence flow, and the rapid distortion RNG k-ε turbulence model was employed. The heat transfer model developed by Han and Reitz [22] was applied to predict the wall heat transfer. The G-equation coupled with the methane chemical reaction mechanism GRI3.0 [23] was used to simulate the flame propagation of natural gas. GRI3.0 mechanism contains 53 species (including argon) and 325 reactions (3 are duplicates because the sum of two rate parameter expressions is required). The spark event was simplified by a 0.5 mm spherical passive source centered on the spark plug gap.

The accuracy of the 3D numerical model established by STAR-CD was comprehensively validated against the measured in-cylinder pressure and the apparent heat release rate as shown in Fig. 4, as well as the ignition delay, CA50 and combustion duration at 1200 rpm as shown in Table 2. It was found that the deviation of the model predicted and experimentally measured maximum in-cylinder pressure was less than 0.3 MPa. The simulated heat release rate also agreed closely with the measurements. In addition, the predicted ignition delay, CA50 and combustion duration also showed good agreement with measurements.

2.2.2. 1D numerical model and validation

GT-SUITE was used to establish the 1D numerical model of the SI natural gas engine in this paper. Various components and reference objects were chosen from the library, after which the selected components were connected appropriately to form an integral 1D simulation model of the turbocharged SI natural gas engine, as presented in Fig. 5.

In this model, the quasi-3D turbulent combustion model named SITurb [24,25] was used to simulate the combustion process of the natural gas engine. The Woschni heat transfer model [6] was adopted to simulate all heat transfer behaviors. Mathematical expressions of the SITurb combustion model and Woschni heat-transfer model are shown in the Table 3.

After the calibration of the 1D numerical model, the accuracy of numerical simulation was subsequently verified by comparing the results of experiment and simulation, in terms of the power and economic performance of the natural gas engine. Fig. 6a and b compare the engine torque and the natural gas consumption rate at the WOT condition from the 1D model prediction and the engine bench tests. Generally good agreement was observed for both the engine torque and the fuel consumption rate at all engine speeds. The maximum deviations between simulations and experiments for the engine power and natural gas consumption rate were 1.2% and 5%, respectively. Therefore, the 1D numerical model established in this paper was used to optimize the intake timing and the intake valve lift.

2.2.3. Hierarchical 1D/3D approach

3D CFD simulations are often used for detailed analysis of in-cylinder flow, charge movement and combustion. However, detailed 3D model is computationally expensive [20]. Therefore, hierarchical 1D/3D approach is adopted in this work to predict combustion and in-cylinder flow with less time consuming. Fig. 7 shows how the 1D/3D model is coupled for the present simulation. Firstly, 3D CFD simulations without combustion process was employed to provide detailed information of the kinetic energy (K), turbulent kinetic energy (k) and turbulence integral length scale (ε) within the whole intake and compression stroke. Secondly, the quasi 3D turbulent flame combustion model SITurb was used to calculate the combustion process of natural gas engine. After the

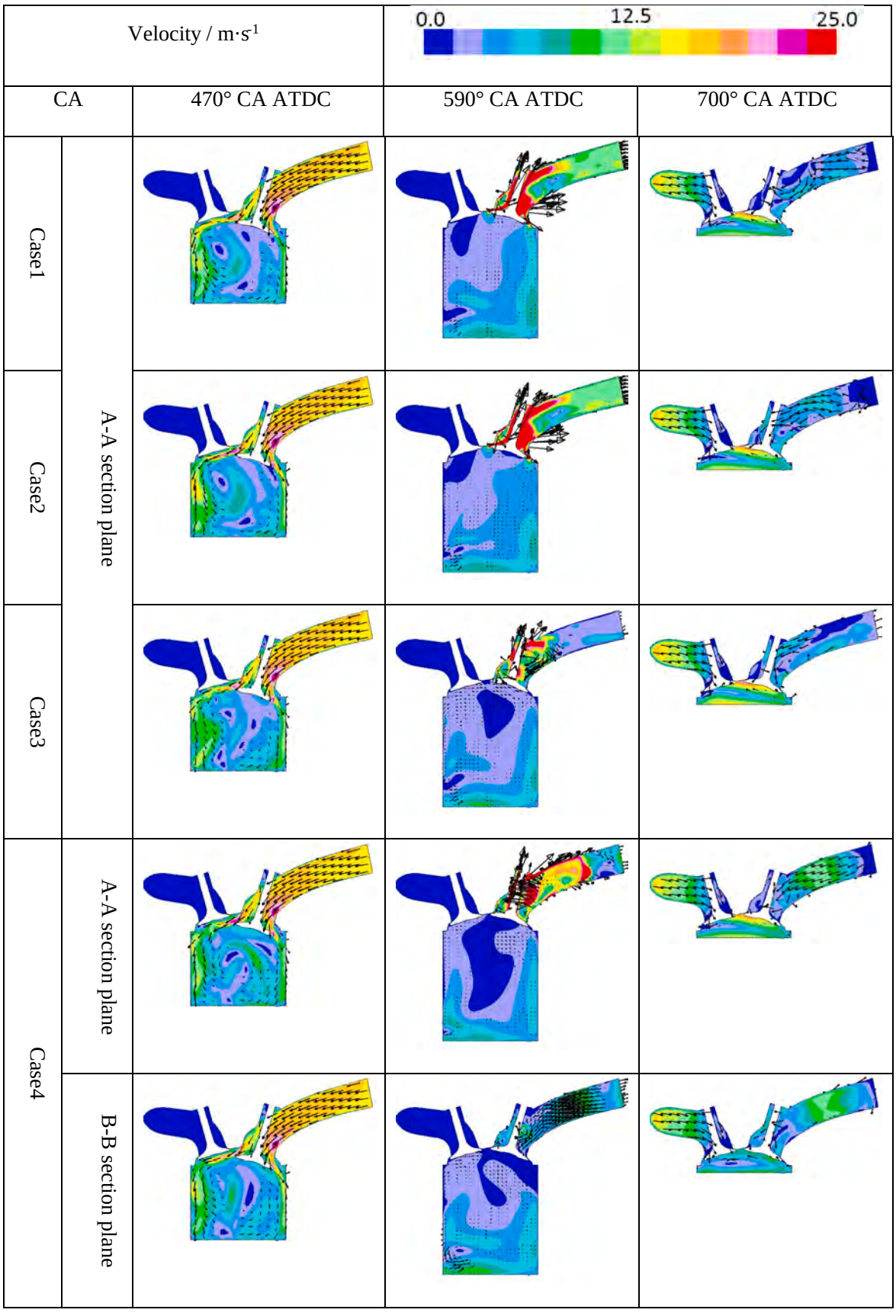

Fig. 11. Comparison of velocity under different cases at 1200 rpm.

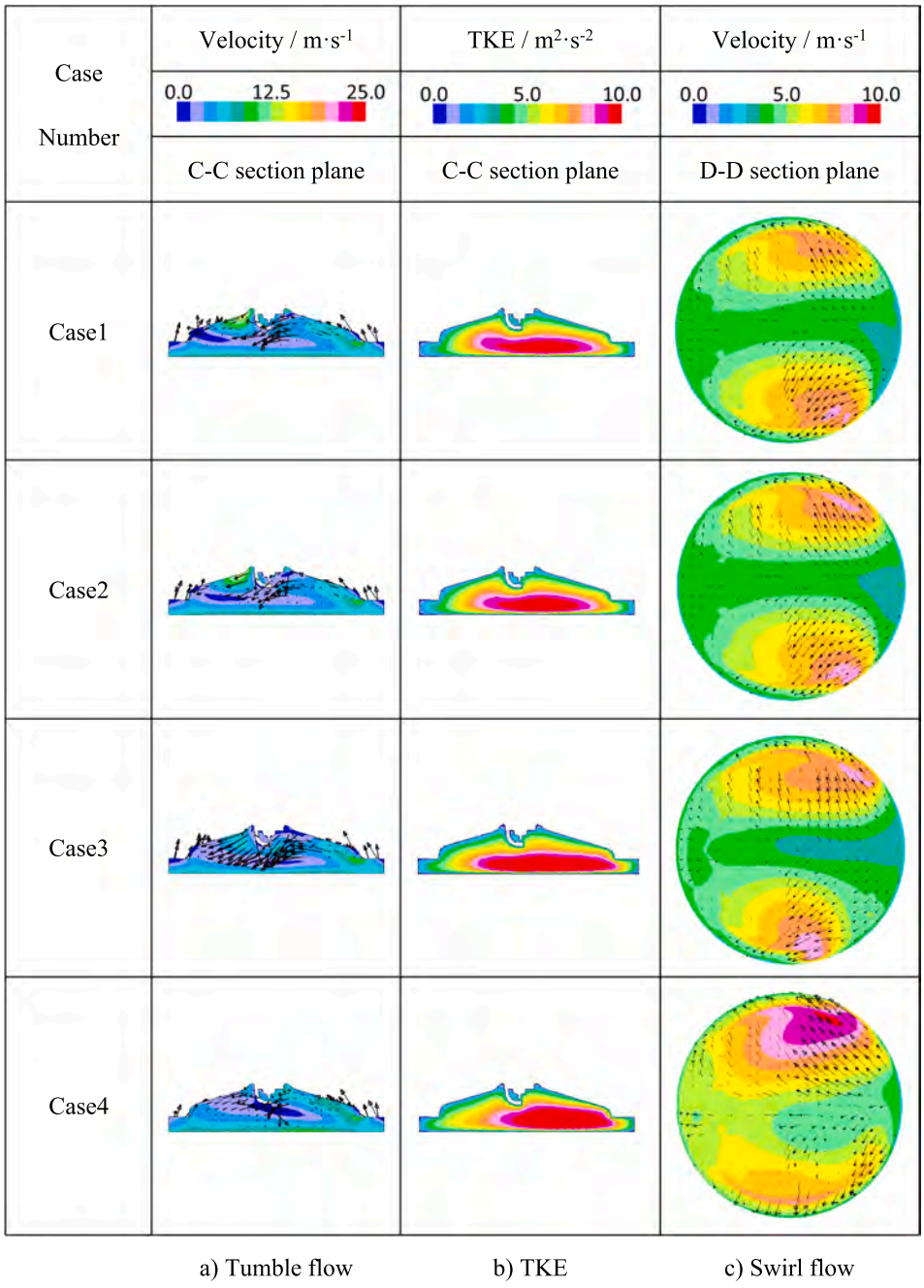

Fig. 12. Comparison of in-cylinder tumble flow, turbulent kinetic energy and swirl flow at spark timing (700° CA).

optimization, several different intake timing strategies were proposed. Finally, a 3D CFD simulation with combustion process was used to analyze the in-cylinder flow and combustion process of each intake timing strategy.

2.3. Numerical setup of different intake strategies: Intake timing and valve lift

As is known to all, the volumetric efficiency of the engine is greatly affected by the valve timing. If the intake valves close timing is too advanced or delayed, it will have a negative influence on the volumetric efficiency. Based on the original engine at the WOT condition, simulation results of the intake mass flow rate and in-cylinder mass versus crank angle under different engine speeds are shown in Fig. 8.

At the engine speed of 1200 rpm, before TDC (351° CA), the intake valve opens and then both the mass flow rate and the in-cylinder mass increase gently. At approximately 410° CA, the mass flow rate reaches the maximum value because the intake valve lift peaks at around this crank angle (as shown in Fig. 2b). After that, the mass flow rate decreases to zero at 550° CA and the total cylinder mass reaches its maximum. Then the mass flow rate becomes negative, which indicates that there is a backflow into the intake port. At higher engine speeds, similar mass flow behaviors are observed. However, as the engine speed increases to 4000 rpm, the peak mass flow rate increases because of the higher intake pressure due to the increased turbo speed. Backflow is also observed. In addition, for different engine speed conditions, in-cylinder mass all reaches a maximum at around 550° CA. When the engine speed is further increased to 5200 rpm, the cylinder mass decreases compared to the 4000 rpm case. This is because at the engine speed of 5200 rpm, the intake pressure is limited. For all the engine speed conditions, an

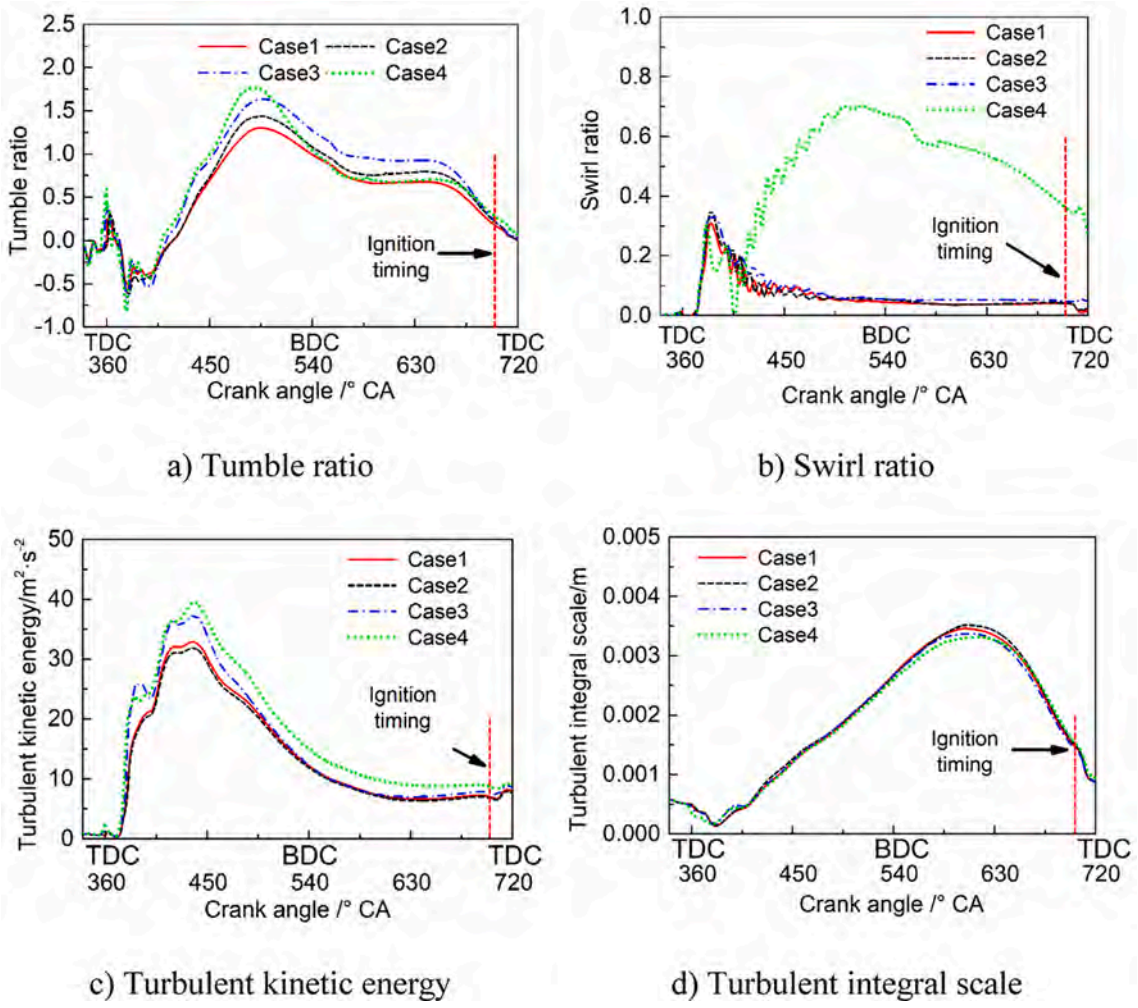

Fig. 13. The variations of swirl ratio, tumble ratio, average turbulent kinetic energy and turbulent integral scale of in-cylinder flows with crank angles.

obvious decrease of the cylinder mass is observed, and the backflow is evident. This backflow results from the late intake valve close timing of the original engine will decrease the volumetric efficiency, and it is believed to reduce the engine torque.

Based on the above analysis, we have designed three new intake timing strategies. These were done by combining different intake parameters, including the intake timing and maximum valve lift, as shown in Table 4 and Fig. 9. All these cases have the same IVO (351° CA). Cases 2 and Cases 3 have synchronized timing and lift for the two intake valves, while Case 4 has asynchronized timing and lift for intake valve 1 and 2. Compared to the original intake timing in Case 1, Case 2 has a lower maximum valve lift (8.59 mm) but with the same IVC (619° CA). Case 3 has the same valve lift as Case 2, but an earlier IVC (591° CA). For Case 4, intake valve 1 has the same IVC (591° CA) as Case 3, but the intake valve 2 has an even earlier IVC (579° CA). We also note that because we focus on the intake strategy, the exhaust valve timing and lift for all the cases are fixed as shown in Fig. 2b.

3. Numerical results and discussion

Based on the numerical approaches in Sec. 2.2 and the designed intake strategies in Sec. 2.3, we have simulated the intake mass flow rate, the in-cylinder flow during the intake and compression process, as well as the temperature distribution, in-cylinder pressure and heat release rate for the combustion and expansion process.

3.1. Intake mass flow rate and in-cylinder mass

Simulation results of the intake mass flow rate and in-cylinder mass with different intake strategies are presented in Fig. 10. At high and intermediate engine speeds (5200, 4000 and 2000 rpm), different intake strategies lead to the similar mass flow rate and in-cylinder mass, except for the period of IVC delay (Crank angle between BDC and IVC). However, at the low engine speed of 1200 rpm, reducing the intake duration and using the asynchronized intake timing strategy (Case 4) significantly increases the in-cylinder mass and reduces the backflow, as shown by the Fig. 10d. Specifically, the in-cylinder mass after IVC is increased by 35%, compared to the original strategy (Case 1). In addition, it should be noted that there is no such backflow phenomenon for Case 3 and Case 4 for all the engine speeds. The main reason is that the durations of intake valve opening of Case 3 (240° CA) and Case 4 (240° CA of intake valve 1, 224° CA of intake valve 2) are shorter than those of Case 1 and Case 2 (264° CA). Furthermore, it can be observed that the intake flow rate fluctuation at this engine speed is the most severe.

3.2. In-cylinder flow during the intake and compression process

Since the intake strategy has the most significant influence at 1200 rpm, we then focus on the in-cylinder flow behaviors under different intake strategies at 1200 rpm. As shown in Fig. 11, the intake duration of Case 4 is shortened, and one of the intake valves has almost no backflow, which weakens the backflow phenomenon in the compression stroke.

Fig. 12 shows the comparison of in-cylinder tumble flow, turbulent

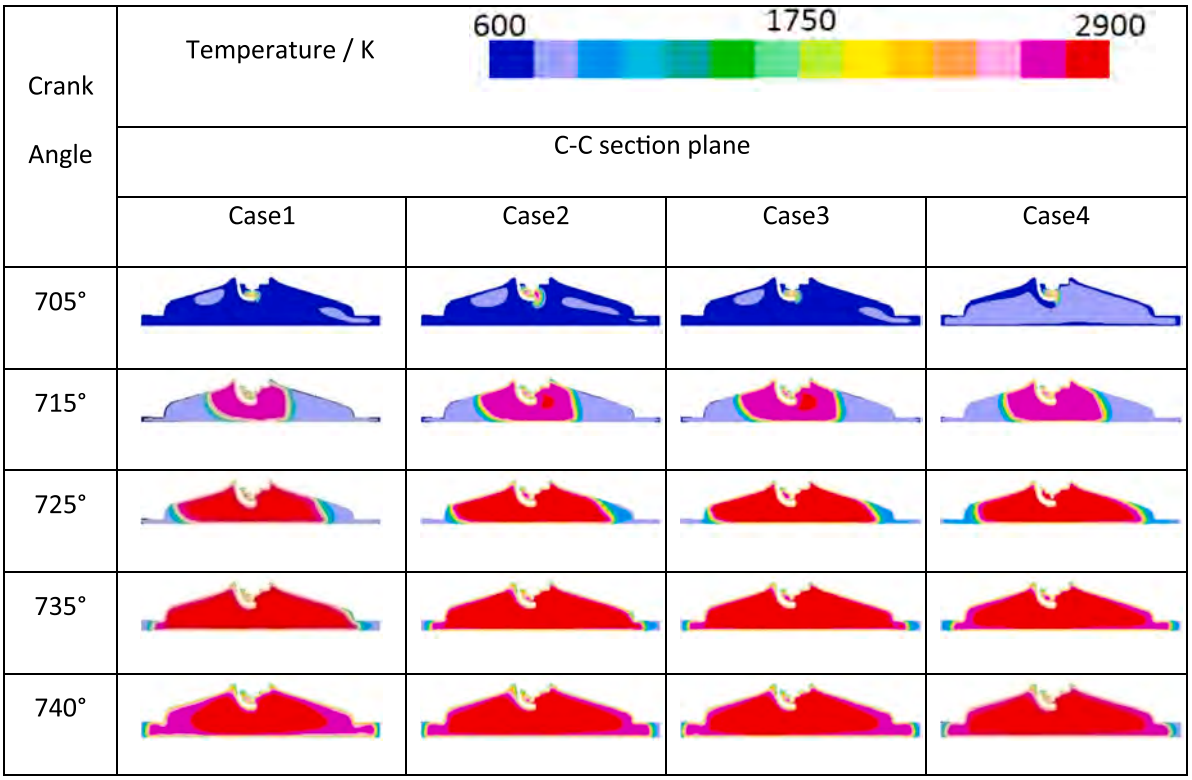

Fig. 14. Comparison of temperature distribution of different strategies at 1200 rpm.

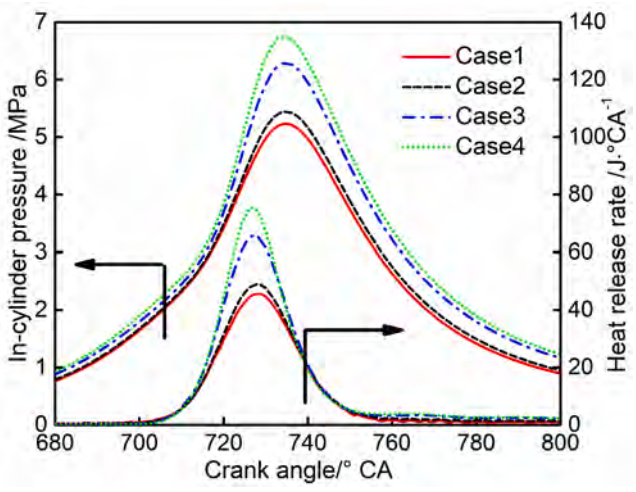

Fig. 15. Comparison of in-cylinder pressure and heat release rate.

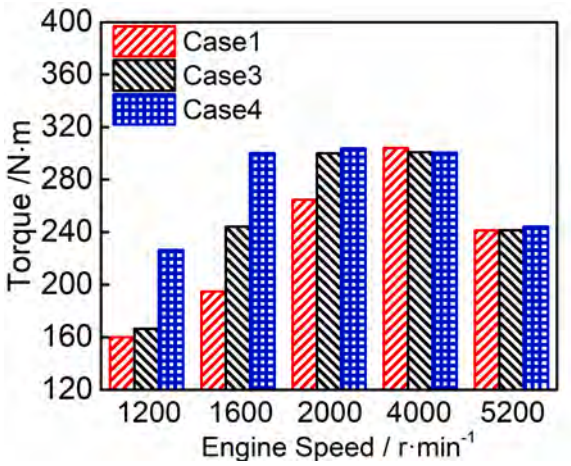

Fig. 16. Comparison of torque results of each strategy.

kinetic energy and swirl flow at spark timing on a section plane cutting the spark plug and parallel to the cylinder axis (C—C section plane), under different cases at 1200 rpm. From Fig. 12a, a tumble-promoting flow pattern can be recognized for all the cases, which promotes the turbulent kinetic energy at spark timing (700° CA). As shown in Fig. 12b, the turbulent kinetic energy in Case 4 is the largest, with the strongest vortex formed in the compression stroke and the highest turbulent kinetic energy generated at the end of compression. Moreover, as seen in Fig. 12c, a larger swirl ratio is generated in Case 4 because of the asynchronized intake valve lift which breaks the symmetry of the intake flow.

The influence of the intake strategy on the tumble ratio, swirl ratio, turbulent kinetic energy, and turbulent integral scale of in-cylinder flows are comprehensively studied at the engine speed of 1200 rpm, as presented in Fig. 13. Fig. 13a shows that for Case 1 (the original intake strategy) and Case 2, the tumble ratios are similar. For Case 3 and Case 4, the tumble ratios are slightly increased in the intake process. In addition, the peak tumble ratio is advanced for Case 4. Fig. 13b shows that for the synchronized intake strategies (Case 1, 2 and 3), very similar swirl ratios are observed. While for Case 4, large swirl ratio is generated because of the asynchronized intake valve lift which breaks the symmetry of the intake flow. The intake valve 1 in Case 4 has the same IVC (591° CA) as that in Case 3, but its intake valve 2 has an even earlier IVC (579° CA). Such asynchronized intake strategy will lead to the asymmetric flow motion in two intake ports, which is beneficial for the generation of stronger swirl flow in the in-cylinder charge. The difference of the in-cylinder swirl flow between case 4 and other cases is more obvious in Fig. 12c. Fig. 13c shows that the variation of turbulent kinetic energy in cylinder is similar for Case 1 and 2. TKE in Case 3 and Case 4 are higher.

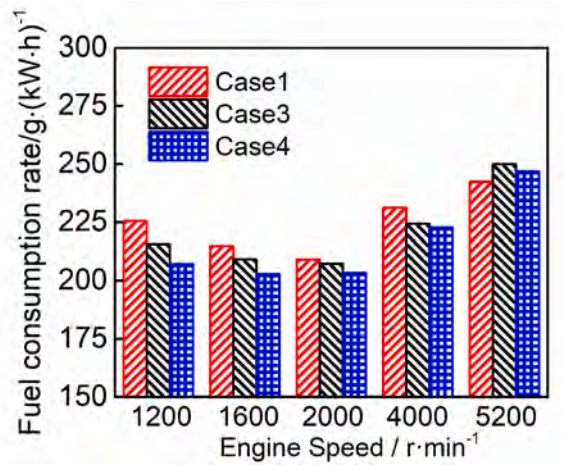

Fig. 17. Comparison of natural gas consumption rate of each strategy.

As it approaches the spark ignition at TDC, the TKE in Case 4 is the largest. This is because the swirl ratio of Case 4 is higher than other cases at the later stages of the intake stroke and the compression stroke. These large-scale swirls are converted to turbulence due to compression at TDC, resulting a higher TKE for Case 4 at TDC. This higher TKE for Case 4 will have a positive influence on the turbulent flame speed and will lead to higher thermal efficiency [26]. Fig. 13d shows that the turbulent integral scale of each intake strategy is similar. In addition, the turbulent integral scale peaks at approximately the intake valves close timing for each intake strategy.

3.3. Combustion process analysis

We further compared the combustion characteristics during the combustion process for different intake strategy cases, including the flame kernel growth and propagation, the temperature distribution, and the overall pressure and heat release based on the 3D simulations. The engine speed is also fixed at 1200 rpm.

3.3.1. Temperature distribution

Fig. 14 compares the temperature distribution evolution in the combustion chamber near TDC. When the spark ignites at 700° CA, a high temperature region is generated at the electrodes gap and propagates outwardly. Compared with Case 1 (the original intake strategy), the in-cylinder temperature at the spark ignition for Case 4 is approximately 60 K higher, which is expected to lead to higher laminar flame speed (S_L in Eq. 1). In addition, since TKE is the largest in Case 4 (Fig. 13), there is the strongest vortex formed in the compression stroke and the highest turbulent kinetic energy generated at the end of compression. This increased turbulent intensity u', leads to a higher turbulent flame speed (S_T in Eq. 2), and ultimately results in higher flame propagation speed (dM_b/dt). This is evidenced by the slightly larger high temperature region as well as the high temperature region area evolution (T greater than 1800 K) profiles. It indicates that the flame propagation is accelerated and the combustion duration is decreased for Case 4. As such, the combustion is closer to a constant volume one and expected to a higher indicated thermal efficiency.

3.3.2. Pressure and heat release rate

Fig. 15 shows the comparison of the in-cylinder pressure and heat release rate at 1200 rpm for different intake strategies. It can be seen that, compared with Case 1 (the original intake strategy), the maximum in-cylinder pressure for Case 2, 3 and 4 intake strategy is 4.1%, 20.3 %, 28.9 % higher, respectively. The heat release rate curves of different intake strategies are similar. Compared with Case 1, Case 2 has a slight increase in the heat release rate due to smaller intake valve lift. Based on Case 2, the intake duration of Case 4 and 3 is reduced, the peak values of the heat release rate are obviously larger, and the combustion phase is slightly advanced. As the intake flow rate increases, more intake charge is introduced before the IVC, and higher total pressure is expected. In addition, because of the higher flame burning rate during flame propagation, the heat release rate is also increased. As such, the thermal efficiency of the engine is increased. Furthermore, compared with Case 3, Case 4 has asynchronous intake timing, in which one intake valve has a shorter intake duration and shorter valve lift. This can effectively improve the swirl ratio in the cylinder (Fig. 13b) and the TKE at the spark ignition (Fig. 13c), which further increases the heat release rate.

4. Engine tests with optimized intake strategies

Based on the above simulations, we believe the intake strategy in Case 4 is the optimized one for the present engine. Therefore, we designed cam profiles according to the intake strategy of Case 3 and Case 4, and then conducted engine performance tests at the low engine speeds (1200 rpm, 1600 rpm and 2000 rpm), the maximum torque speed (4000 rpm), and the rated speed (5200 rpm). As shown in Fig. 16, the engine torque in Case 3 and Case 4 is increased for all the engine speed conditions, compared with the original strategy in Case 1. At the engine speeds of 1200, 1600, 2000, and 4000 rpm, the engine torque improvements for Case 3 intake strategy are 3.91%, 25.34%, 13.31%, and −0.01%, respectively. For Case 4 intake strategy, the torque improvements are even more (41.42%, 54.10%, 14.81%, and −0.02%). We also note that at the highest engine speed (5200 rpm), the engine torque for each intake strategy is reduced compared to 4000 rpm due to the lower volume efficiency (Fig. 8). However, the Case 4 intake strategy still has a slight torque improvement compared to the original one at this high speed.

For the fuel consumption rate, Fig. 17 compares the experimental results for different cam profiles. Compared with the original engine, the BSFC for Case 3 intake strategy at the engine speed of 1200, 1600, 2000, and 4000 rpm is respectively 9.8, 5.7, 1.8, and 6.9 g/kW·h decreased. For Case 4 intake strategy, the BSFC saving are even more attractive (respectively 18.3, 12.0, 5.7, and 8.5 g/kW·h). At highest engine speed (5200 rpm), Case 3 and Case 4 slightly increases the BSFC, while this is acceptable because it is a less frequent engine speed condition.

5. Conclusions

Effects of different intake strategies on a turbocharged SI natural gas engine with 4 valves (2 intake valves and 2 exhaust valves) were investigated numerically and experimentally. Results show that the asychornized intake strategy with shorter intake valve lift but earlier intake valve closing is the optimized one since it increases the low-speed engine torque and reduces the brake specific fuel consumption remarkably. Specifically, a hierarchical 1D/3D approach was proposed to simulate the intake flow, the gas motion during compression, the flame kernel growth and temperature distribution during combustion, and ultimately the combustion pressure and heat release rate evolutions for all the designed intake strategy cases. Numerical simulation shows that the asychornized intake strategy increases the volumetric efficiency and turbulent kinetic energy before ignition, which increases the flame propagation and leads to higher peak pressure and heat release rate. This optimized intake strategy is correspondingly applied to the test engine, and engine dyno experiments show that the torque is increased and brake specific consumption rate is reduced remarkably, especially at the low engine speed condition.

Declaration of Competing Interest

The authors declare that they have no known competing financial interests or personal relationships that could have appeared to influence the work reported in this paper.

Acknowledgement

This work was supported by the National Key Research and Development Program of China (No. 2018YFB0105900).

References

[1] Cho HM, He BQ. Spark ignition natural gas engines-A review. Energy Convers Manage 2007;48(2):608–18. https://doi.org/10.1016/j.enconman.2006.05.023.
[2] Zheng J, Chen X, Hu T, Zhan Z. The Research Development in Direct Injection Spark-Ignition Natural Gas Engine. Lecture Notes in Electrical Engineering 2013; 191:51–63. https://doi.org/10.1007/978-3-642-33777-2_5.
[3] Nwafor OMI. Effect of advanced injection timing on emission characteristics of diesel engine running on natural gas. Renewable Energy 2007;32(14):2361–8. https://doi.org/10.1016/j.renene.2006.12.006.
[4] . S, Bakar RA, Ismail AR. Green Engines Development Using Compressed Natural Gas as an Alternative Fuel: A Review. American journal of environmental sciences 2009;5(3):371–81.
[5] Bayat Y, Ghazikhani M. Experimental investigation of compressed natural gas using in an indirect injection diesel engine at different conditions. J Cleaner Prod 2020;271. https://doi.org/10.3844/j.jclepro.2020.122450.
[6] Heywood J. Internal Combustion Engine Fundamentals. McGraw-Hill; 1988.
[7] Bhandari K, Bansal A, Shukla A, Khare M. Performance and emissions of natural gas fueled internal combustion engine: A review. Journal Ofentific & Industrial Research 2005;64(5):333–8. https://doi.org/10.1088/0960-1317/5/029.
[8] Kato K, Igarashi K, Masuda M, Otsubo K, Yasuda A, Takeda K, et al. Development of Engine for Natural Gas Vehicle. SAE Technical Paper Series 1999.
[9] Suple PJ, Sonawane CR, Thipse SS, Mohite JP, Chougule NB, Pandey A. Low Engine Speed Torque Improvement in Natural Gas Engine: Experimental Observations. Process Integration and Optimization for Sustainability 2020;4(4):429–44. https://doi.org/10.1007/s41660-020-00131-w.
[10] Ibrahim A, Bari S. An experimental investigation on the use of EGR in a supercharged natural gas SI engine. Fuel 2010;89(7):1721–30. https://doi.org/10.1016/j.fuel.2009.07.005.
[11] Thipse SS, Dsouza A, Sonawane SB, Rairikar SD, Kavathekar K, Marathe N, et al. Development of Multi Cylinder Turbocharged Natural Gas Engine for Heavy Duty Application. SAE Int J Engines 2017;10(1):27–38.
[12] Luisi S, Doria V, Stroppiana A, Millo F, Mirzaeian M. Experimental Investigation on Early and Late Intake Valve Closures for Knock Mitigation through Miller Cycle in a Downsized Turbocharged Engine. SAE Technical Paper Series 2015. https://doi.org/10.4271/2015-01-0760.
[13] Highly FM, Engines ENG. SAE Technical Paper Series 2017. https://doi.org/10.4271/2017-24-0059.
[14] Zhang S, Li Y, Wang S, Zeng H, Liu J, Duan X, et al. Experimental and numerical study the effect of EGR strategies on in-cylinder flow, combustion and emissions characteristics in a heavy-duty higher CR lean-burn NGSI engine coupled with detail combustion mechanism. Fuel 2020;276:118082.
[15] Bhasker JP, Porpatham E. Effects of compression ratio and hydrogen addition on lean combustion characteristics and emission formation in a Compressed Natural Gas fuelled spark ignition engine. Fuel 2017;208:260–70. https://doi.org/10.1016/j.fuel.2017.07.024.
[16] Sabaruddin AA, Wiriadidjaja S, Shakrine AM, Rafie D, Jojodihardjo H. Engine optimization by using variable valve timing system at low engine revolution. ARPN Journal of Engineering and Applied Sciences 2015.
[17] Jung J, Song S, Hur KB. Numerical study on the effects of intake valve timing on performance of a natural gas-diesel dual-fuel engine and multi-objective Pareto optimization. Appl Therm Eng 2017;121:604–16. https://doi.org/10.1016/j.applthermaleng.2017.03.036.
[18] Lee K, Bae C, Kang K. The effects of tumble and swirl flows on flame propagation in a four-valve S.I. engine. Appl Therm Eng 2007;27(11–12):2122–30. https://doi.org/10.1016/j.applthermaleng.2006.11.011.
[19] Liu K, Yang J, Jiang Wu, Li Y, Wang Yi, Feng R, et al. Effect of asynchronous valve timing on combustion characteristic and performance of a high speed SI marine engine with five valves. Energy Convers Manage 2016;123:185–99.
[20] Mirzaeian M, Millo F, Rolando L. Assessment of the Predictive Capabilities of a Combustion Model for a Modern Downsized Turbocharged SI Engine. SAE Technical Paper Series 2016. https://doi.org/10.4271/2016-01-0557.
[21] Han Z, Reitz RD. Turbulence Modeling of Internal Combustion Engines Using RNG κ-ε Models. Combust Sci Technol 1995;106(4–6):267–95. https://doi.org/10.1080/00102209508907782.
[22] Han Z, Reitz RD. A temperature wall function formulation for variable-density turbulent flows with application to engine convective heat transfer modeling. Int J Heat Mass Transf 1997;40(3):613–25. https://doi.org/10.1016/0017-9310(96)00117-2.
[23] Gregory PS, David MG, Michael F, Nigel WM, Boris E, Mikhail GC,et al. GRI-Mech 3.0, http://www.me.berkeley.edu/gri_mech/; [accessed 24 April 2021].
[24] De Bellis V, Bozza F, Fontanesi S, Severi E, Berni F. Development of a Phenomenological Turbulence Model through a Hierarchical 1D/3D Approach Applied to a VVA Turbocharged Engine. SAE Int J Engines 2016;9(1):506–19. https://doi.org/10.4271/2016-01-0545.
[25] Zhao J, Xu M. Fuel economy optimization of an Atkinson cycle engine using genetic algorithm. Appl Energy 2013;105:335–48. https://doi.org/10.1016/j.apenergy.2012.12.061.
[26] Wei S, Wang F, Leng X, Liu X, Ji K. Numerical analysis on the effect of swirl ratios on swirl chamber combustion system of DI diesel engines. Energy Convers Manage 2013;75:184–90. https://doi.org/10.1016/j.enconman.2013.05.044.